CBS TECHNOLOGY CENTER

MODELING OF A PIANO HAMMER

MARCH 1, 1985

Hideo Suzuki

CBS Technology Center
227 High Ridge Road
Stamford, CT 06905

MODELING OF A PIANO HAMMER

ABSTRACT

From the measurement of the force-time pattern and the acceleration-time pattern of a piano hammer, the effective mass and the stiffness curve are obtained. Using these values, a hammer model of a single mass-spring system is established. A further improvement of the model is accomplished by employing a double mass-spring system. It is expected that the interaction between a hammer and a string can be more accurately analyzed by using these proposed hammer models.

INTRODUCTION

There is no doubt about the fact that a piano hammer has a great contribution to the total quality of a piano sound. This may be proved by the fact that the sound quality of a piano is finally adjusted by changing the property of the hammer felt at the end of the manufacturing process. It is also a common experience that a piano tone becomes not only louder but also brighter when a key is hit harder. The loudness change can be considered as a result of a larger hammer velocity. On the other hand, the qualitative change of the sound must be attributed to some other factor, possibly nonlinear characteristics of the piano hammer.

In the past, many studies have been conducted on the interaction between a piano hammer and a string.[1-11] Very few papers, however, discuss the nonlinear characteristics of the piano hammer. Among these few is M. Ghosh,[10] who assumed that the compression of a piano hammer obeys Hertz's law at the beginning of the hammer-string contact, and then, after some amount of compression, Hook's law takes over. Even in the recent studies conducted on the hammer-string interaction, the nonlinear characteristic is not considered. K. K. Deb[12] studied the dynamic vibration of a string excited by the impact of a hard mass taking into account the loading of the string by the mass during the period of contact.

T. Yanagisawa et al[13] assumed a coefficient of restitution between a string and a hammer and calculated the time history of the displacement of

the string. I. Nakamura [14] represented a piano hammer by a single mass-spring system (with a constant spring coefficient) and a string by an electrical transmission line, and obtained the force-time pattern using an analog computer.

Establishing a proper model for a piano hammer is important for a comparison of the qualities of different hammers. The model can also be used to theoretically discuss the functions of different parts of a piano in conjunction with the hammer. This author, after a study of different techniques to measure the stiffness of a felt sheet, found that the static and dynamic stiffnesses are different, which indicates the importance of mesuring the characteristics of the piano hammer in a way that is as close as possible to the real situation. This paper discusses how a model of a hammer is established for measurement of a force-time pattern and an acceleration-time pattern using a key-action model. At first, a mass-spring system (with a nonlinear spring constant) of single degree of freedom is investigated as a model. Then, to improve the accuracy of the model, a double mass-spring is considered. In a later section, a convenient way of representing the stiffness characteristic of a piano hammer is discussed.

While this manuscript was being prepared, a dynamic measurement of the compression characteristics of piano hammer felt was reported by T. Yanagisawa and K. Nakamura.[15] They measured the displacement of the string and the felt deformation as a function of time and concluded that a piano hammer must be represented as a distributed mass, spring, and loss system. In the

following sections, however, it will be shown that the dynamic characteristic of a piano hammer is well represented by a one or two degree-of-freedom system.

I. TEST SETUP

The test setup for the measurement of the force-time pattern and an acceleration-time pattern of a hammer is shown in Fig. 1. The hammer used for this measurement was the one corresponding to the 60th note (G# above C5). When the key is struck, the hammer is pushed upward. After a short period of acceleration, the hammer inluding the shank is set free from acceleration and moves upward with almost constant velocity. The top of the hammer hits an attachement which is rigidly connected to a force gauge when the shank is almost parallel to the ground. The top of the attachment has a shape which resembles a single string with a diameter of 1.25 mm. The force gauge is fixed to an L-shaped arm which is strong enough to keep the force gauge unmoved even if it is hit by a maximum force of almost 10 Kg. The force gauge gives an electrical output which is proportional to the applied force as a function of time. (A portion of the wood of the hammer is cut so that the accelerometer can be easily attached to the hammer.) A disadvantage of this measuing system is the fact that the accelerometer is attached to the hammer as an additional mass. The mass of the accelerometer was 2.3g for the first measurement and, then, a lighter accelerometer of 1gr was used. For the present time, however, a modeling of the hammer will be tried considering the mass of the accelerometer as a portion of the mass of the hammer.

The two signals from the transducers are sent to a Structural Dynamics Analyzer (HP-5423A), where they are stored in a tape memory. After the measurement is completed, data is sent to a medium size computer, DEC PDP-11/70, for the analysis.

II. RESULTS AND DISCUSSION

2.1 Force-Time and Acceleration-Time Patterns

The force-time and acceleration-time patterns are measured for five cases from (a) to (e). Measurement (a) corresponds to the hardest strike of the key, and measurement (e) to the softest. The force-time patterns and the acceleration-time patterns are shown in Fig. 2 and Fig. 3, repsectively. The horizontal axis was shifted so that the peaks are located at the same position on the horizontal axis. It is clear that the force and accleration pulses become narrower as the key is struck harder. The importance of this fact is that a force-time pattern with a narrower width contains more energy in the high frequency region than a pulse with a wider width. In a real situation, string's higher partials will be more vigorously excited, when a key is struck harder than when it is struck softer.

The power spectrum of the force-time patterns in Fig. 2 are shown by the curves from (a) to (e) in Fig. 4. The frequency at which the power spectrum decreases by 20 dB from the zero frequency level are 2.17, 1.65 and 0.938 KHz for curves (a), (c) and (e), respectively. The relation of the maximum force,

F_{max}, to the bandwidth, BW, is roughly given by $F_{max} \propto (BW)^3$. Figure 4 clearly indicates that the sound will be much brighter as well as louder when the key is struck harder. This characteristic, which results from the nonlinearity of the hammer flet, is one of the most important characteristics of the piano sound.

The acceleration-time pattern shows some ringing after the main peak. Two reasons for this may be considered. The shank-hammer combination is a resonating system which may have alternating motion as well as a simple strike and return motion. The other is the limitation of the frequency response of the measuring system at the low end. For these reasons, in some of the following discussions, only the left-hand side of the peak of the acceleration-time pattern will be used.

2.2 Force-Displacement Relationship

Once the acceleration A(t) is known, the velocity V(t) and the displacement X(t) are calculated with unknown constants V_o and X_o such as

$$V(t) = \int_{-\infty}^{t} A(t')dt' + V_o \qquad (1)$$

and

$$X(t) = \int_{-\infty}^{t} V(t')dt' + X_o \qquad (2)$$

The constant V_0 is determined so that V(t) becomes zero at the time when A(t) and the force-time pattern F(t) shows their peak. The displacement, X(t), is physically the position of the hammer, and one can choose any position as an origin of X. One of the reasonable choices for this origin is the position of the hammer when it barely touches the force gauge attachment. In this case X(t) is considered as the compression of the felt (if $X(t) \geq 0$). It is not easy in doing this, however, since the surface of the felt is not smooth and it does not have clear boundary.

Another way of determining the origin was found after a careful investigation of the force-displacement relationship of the hammer. When the origin of X is properly chosen, the force-displacement relationship of this hammer is well approximated by $F = KX^4$, where K is a constant. Even if the approximation is not altogether accurate, this condition can still be used to determine the origin. Figure 5 shows the force-displacement relationship obtained from the measurement (a), (b) and (d). It also shows a force-displacement relationship given by a straight line. This will be explained later. The curve shown by the solid line is the calculated force-displacement relationship by $F = 86.9\ X^4$ (Newton vs. mm). It should be mentioned that the measured force-displacement relationships for different hammer velocities are well approximated by a simple approximation of the form $F = KX^4$. For a better approximation, the second and third order terms can also be included such as $F = K_1\ X^2 + K_2\ X^3 + K_3\ X^4$. Actually, the program used for the calculation of the force-displacement relationship has

the capability to use this form. From the force-displacement relationship, $F = KX^4$, the stiffness of the hammer felt $S(X)$ is given by $S(X) = F/X = KX^3$. This is the first step in building an equivalent circuit of a hammer.

2.3 Equivalent Mass of the Hammer

If one assumes that the motion of the hammer during the contact is represented by a mass-spring system as shown in Fig. 6, the equation of motion is given by

$$M_{eff} \cdot \ddot{X}(t) + S(X) \cdot X(t) = -M_{eff} \cdot G, \qquad (3)$$

where M_{eff} is the mass of the system, $S(X)$ is the stiffness of the hammer felt, and G is the gravity constant. Then M_{eff} is given by

$$M_{eff} = \frac{S(X)\ X(t)}{-[\ddot{X}(t) + G]} = \frac{F(t)}{-[\ddot{X}(t) + G]} \ . \qquad (4)$$

For a single mass-spring system to be valid as a hammer model, the equivalent mass obtained from Eq. (4) using the measured force- and acceleration-time patterns must be constant during the entire period of contact. To determine whether this is the case, M_{eff} was calculated as a function of time for measurements (a), (b) and (d), and plotted in Fig. 7.

The force-time patterns are also shown by dotted lines in Fig. 7 for comparison (the vertical axis for the force is not shown). The results show that M_{eff} is almost constant during the time when the hammer is moving upward, except at the very beginning. Also, M_{eff} has a very small dependence on the initial velocity. The hammer, in the present case, can be said to have a mass of approximately 6.8g.

2.4 Simulation by a Single Mass-Spring System

In order to see how good the single mass-spring system can simulate the motion of the hammer, the force-time patterns were calculated using M_{eff} = 6.8g and $S(X) = 86.9\ X^3$ (Newton/mm) for three cases with initial velocities V_I = 2.1, 1.55 and 0.77 M/sec. These are the measured initial velocities for the measurements (a), (b) and (d), respectively. (The solution of the nonlinear differential equations are shown in the next section.) The results are shown in Fig. 8. The solid lines are the calculated force-time patterns, and the dotted lines are the measured ones. The agreement of the force-time patterns between calculated and measured results are fairly good. The big differences, however, are seen around the peaks and the tails of the curves. The difference between the peak levels of the calculated and measured force-time patterns are 14% for the measurement (a). It was confirmed that if a small initial velocity is used, a much better agreement between the two curves is achieved. With a smaller initial velocity the maximum force becomes low and the pulse becomes wider. An improvement of the accuracy of the measurement system may help reduce the difference. It should be noted,

however, that a real hammer is a much more complicated system than a single mass-spring system. For this reason, some amount of error between the measured and calculated force-time patterns will always exist even if an ideal measurement system were used.

2.5 Simulation by a Double Mass-Spring System

One way to take care of the discrepancy found in the previous section is to add another degree of freedom to the system. A new model of a double mass-spring system is shown by Fig. 9 (a). Figure 9 (b) shows the equivalent electrical circuit for the mechanical system of Fig. 9 (a). The stiffness S_2 can be nonlinear, but for the present case, it is assumed to be linear for simplicity.

The equations describing the motion of this system are

$$M_1\ddot{X}_1 + S_2 \cdot (X_1-X_2) + S_1(X_1) \cdot X_1 = -M_1G \qquad (5)$$

$$M_2\ddot{X}_2 + S_2 \cdot (X_2-X_1) = -M_2G \qquad (6)$$

These nonlinear differential equations are easily solved by the finite difference method. The acceleration $\ddot{X}$ is represented by

$$\ddot{X}(m) = [X(m\pm1) - 2X(m) + X(m-1)]/h^2 \qquad (7)$$

where h is the incremental time and X(m) is the value of X at t = mh (m is the integer). Then Eqs. (5) and (6) are represented as follows:

$$X_1(m+1) = -Gh^2 + [2 - (S_1(X_1) + S_2)h^2/M_1]\, X_1(m) - X_1(m-1) + [S_2h^2/M_1]\, X_2(m), \tag{8}$$

$$X_2(m+1) = -Gh^2 + [S_2h^2/M_2]\, X_1(m) + [2 - S_2h^2/M_2]\, X_2(m) - X_2(m-1). \tag{9}$$

The initial conditions are

$$X_1(0) = X_2(0) = 0 \tag{10}$$

and

$$X_1(-1) = X_2(-1) = V_Ih, \tag{11}$$

where V_I is the initial hammer velocity.

The recurrance formulas Eqs. (8) and (9) give all the values for $X_{1,2}(m)$, $m \geq 1$.

To obtain an optimum set of parameters, every parameter in Fig. 9 (a) can be changed. The optimum set of parameters, in this case, is that set for which the squared error E, which is defined below, becomes minimum

$$E = \sum_{m=o}^{M} (F_{cal} - F_{meas})^2, \tag{12}$$

where F_{cal} is the calculated force-time pattern and F_{meas} is the measured force-time pattern. It is possible to change all the parameters one by one and find a best fitting set of parameters. The problem is that E converges to different values (minima) when the optimizing routine starts with different initial values. If one has two sets of parameters which give a similar amount of E, he cannot tell which one he should choose. To avoid this problem, one must restrict the freedom of some of the parameters.

In Section 2.2 it was found that the force-displacement relationship is well approximated in the form $F = KX^4$ for all cases of measurements. Thus, the stiffness obtained in this way seems reliable and should not be changed. The effective mass M_{eff} was constant in the wide region of the left side of the pulse. This value should also be kept unchanged. For simplicity, it will be assumed M_{eff} is equal to $(M_1 + M_2)$. The remaining freedoms left now are how to determine the ratio of M_1 to M_2 (or $R = M_1/M_{eff}$), and the absolute value of S_2. With only two variables, it is very easy to find an optimum set of parameters. In our calculation, E was computed for the case of the measurement (a) in the range of $0.50 \leq R \leq 1.00$ and $0.1 \leq S_2 \leq 100$ (N/mm). The values of R and S_2 were taken as the ones which gave the smallest E.

Figure 10 shows the results of the force-time patterns calculated by the method described above. The parameters are $S_1 = 86.9\ X^3$ (Newton/mm), $M_1 = 5.0$g, $M_2 = 1.8$g, and $S_2 = 17.2$ N/mm. The force-displacement frelationships due to the stiffness S_1 and S_2 are shown in Fig. 5 by solid lines. Three measured initial velocities $V_I = 2.11$, 1.55 and 0.77 M/sec

were used for the comparison between the measured force-time patterns and the calculated force-time patterns using the model Fig. 9 (a). Figure 10 shows that the measured and calculated results are in good agreement. A major improvement from Fig. 8 is observed around the peak. The differences of the maximum forces between measured and calculated values are very small. There still exists quite a significant difference at the end of the pulse. For the simulation of the force-time pattern of a real piano hammer, however, the "double mass-spring" system of Fig. 9 (a) seems to be a good model.

2.6 Incremental Stiffness as a Function of Force

In Section 2.2 the difficulty of determining an origin for the displacement axis was discussed. To avoid this problem, it was suggested to choose the origin so that the force-displacement relationship can be expressed in a form $F = KX^4$ with a minimum square error. The remaining errors can be taken care of by lower order terms. For a comparison of the stiffness characteristics between different hammers, however, this criterion is not appropriate since the foce-deformation relationship is rather arbitrarily shifted on the X-axis by choosing different origins. In this case, it is much more convenient to use an incremental stiffness $s = dF/dX$ as a function of F to avoid this problem.

Different hammers A, B and C for key number 3 (note B0) were measured using the test setup shown in Fig. 1 with an attachment of larger diameter (5mm). Also, a much lighter accelerometer (1 gr) replaced the previous one. From the measurement of the force-time and acceleration-time patterns, the

incremental stiffnesses s(F) were calculated. Only the left-hand side of the pulses were used as in the previous sections. The results are shown in Fig. 11. Hammer (a) stays stiffer than the other two for the entire range of the force measured. The hammer (C) is the softest of all. Hammer (B) shows interesting characteristics compared to the other two hammers. For a soft touch, hammer (B) may sound similar to the hammer (A) or even brighter. For a harder touch, however, the tone may not be as bright as hammer (A). the results indicate that s(F) can clearly show the differences in stifness characteristics among different hammers without the difficulty in the choice of origin.

The force-displacement relationships (Newton vs mm) for the hammers A, B and C are represented by

$$F_A = -21.5X^2 + 45.0X^3 + 41.4X^4,$$
$$F_B = -40.6X^2 + 71.7X^3 + 32.6X^4, \qquad (13)$$
$$F_C = -10.9X^2 + 15.8X^3 + 18.0X^4,$$

respectively. The above equations show that the lower (2nd and 3rd) nonlinear terms cannot be omitted when approximating the force-displacement relations of these hammers. This indicates that, as a general procedure for hammer modeling, all three terms should be included in the simulation of a force-displacement relationship (and, consequently, the stiffness curve).

III. CONCLUSION

From the measurement of the force-time pattern and the acceleration-time pattern a simple model that describes the action of the hammer, when it hits an ideally rigid string, was established.

Firstly, it was found that the relation between the force and the displacement is well approxiamted by the form $F = KX^4$ for the specific hammer used for the measurement. This shows that the hammer stiffness $S(X)$ has a nonlinearity of the third order. Secondly, the effective mass M_{eff} was calculated using a single mass-spring system model. It is fairly constant during the time when the hammer is moving toward the string. The force-time patterns of this model were calculated using $S(X)$ and M_{eff} for measured initial velocities V_I. The differences of the maximum force between calculated and measured results were approximately 15%.

As a second model, a double mass-spring system was discussed in order to account for the error that was found when using the single mass-spring model. The rate of the masses (keeping the total mass equal to M_{eff}), and the stiffness between the two masses (see Fig. 9 (a)) were determined so that they gave a best fit of a simulated curve to a measured curve. The force-time patterns calculated from this model were in good agreement with measured curves except for a small difference around the end of the pulse.

A representation of stiffness characteristics by an incremental stiffness as a function of force was suggested for the comparison of characteristics

among different hammers. Three different types of hammers were measured, and the differences of stiffness characteristics were clearly shown by using this representation.

A modeling of a piano hammer was performed for a limited number of hammers. The form of the nonlinearity of the stiffness ($S = K_1X + K_2X^2 + K_3X^3$) and the consistency of the effective mass must be checked for many different hammers. The effect of the shape of the attachment simulating an ideally rigid string (or strings) on the force-displacement pattern should also be discussed. The measuring technique needs to be improved so that it does not affect the motion of the hammer. Obviously, a piano hammer has a hysteresis characteristic which was not considered in this paper. By taking into account this phenomenon, a model can be improved to give a better fit especially around the tail of the force-time pattern. These are the problems left as a future work for the further improvement of the piano hammer model. A good model of a piano hammer will help us better understand the interaction between the hammer and the string, and will thus contribute toward improving the quality of the piano as a whole.

ACKNOWLEDGEMENTS

The author would like to acknowledge the helpful daily discussion with his colleagues, Gordon Ebbitt and William Strong. The author would also like to thank the encouragement of Louis Abbagnaro, Robert Finger and Emil Torick, Directors of the CBS Technology Center in pursuing this project. He further wants to express his gratitude to KathleneAnne Reilly for her quick and flawless typing and editing work.

REFERENCES

1 H. L. F. Helmholtz, On the Sensation of Tone , (Dover Publications, Inc., New York, 1954).

2 W. Kaufmann, "Uber die Bewegungen geschlagener Klaviersaiten", Ann. Phys., 54, 674-72 (1895).

3 W. H. George, "On the Helmholtz Theories of the Struck String", Phil. Mag., 6(47), 591-602 (1924).

4 S. Bhargava and R. N. Ghosh, "Elastic Impact of Pianoforte Hammer", Phil. Mag., 6(47), 1141-1149 (1924).

5 W. H. George, "On the Helmholtz Theories of the Struck String, Part II, Experimental", Phil. Mag., 6(48), 34-49 (1924).

6 S. Bharagave and R. N. Ghosh, "On the Elastic Impact of the Pianoforte hammer, Part II", Phil. Mag., 6(49), 121-129 (1925).

7 W. H. George and H. E. Beckett, "The Energy of the Struck String - Part I", Proc. Roy. Soc., A114, 111-139 (1927).

8 W. H. George and H. E. Beckett, "The Energy of the Struck String - Part II", Proc. Roy. Soc., A116, 115-140 (1927).

9 D. Banerji and R. Ganguli, "The Duration of Contact Between the Pianoforte String and a Hard Hammer", Phil. Mag., 7(7) 345-352, (1929).

10 M. Ghosh, "On the Hertzian Impact of an Elastic Hammer on a Damped Pianoforte String," Phil. Mag., 7(17), 521-544 (1934).

11 N. Davy, J. H. Littlewood, and M. McCaig, "The Force-Time Law Governing the Impact of a Hammer on a Stretched String", Phil. Mag., 7(27), 133-143 (1939).

12 K. K. Deb, "Dynamics of the Pianoforte String and Hammer", J. Sound & vib., 20(1), 1-7 (1972).

13 T. Yanagisawa, K. Nakamura, and I. Shirayanagi, "Vibration Analysis of Piano String and Soundboard by Finite Element Method", J. Acoust. Soc. Jpn., 31(11), 661-666 (1975, in Japanese).

14 I. Nakamura, "The Vibration of a Struck String -- Acoustical Research on the Piano, Part I", J. Acoust. Soc. Jpn., 36(10), 504-512, (1980, in Japanese).

15 T. Yanagisawa and K. Nakamura, "Dynamic compression characteristics of piano hammer felt", J. Acoust. Soc. Jpn., 40(11), 725-729, (1984, in Japanese).

CAPTIONS

Fig. 1 Test setup used for the measurement.

Fig. 2 Force-time patterns (a-e) for different hammer speeds.

Fig. 3 Acceleration-time patterns (a-e) for different hammer speeds.

Fig. 4 Power spectra of the force-time patterns shown in Fig. 2.

Fig. 5 Measured and simulated force-displacment relationships.

Fig. 6 Singla mass-spring model of a hammer.

Fig. 7 Calculated effective masses using Eq. (4) for measurements a, b and d (solid lines). The measured force-time patterns are also shown (dotted lines).

Fig. 8 Measured (dotted line) and simulate (solid line) force-time patterns for measurements a, b and d. The single mass-spring system is used as a hammer model.

Fig. 9 Double mass-spring system model of a hammer.

Fig. 10 Measured (dotted line) and simulted (solid line) force-time pattern for measurements a, b and d. The double mass-spring system is used as a hammer model.

Fig. 11 Incremental stiffness curves of three different hammers A, B and C as a function of force.

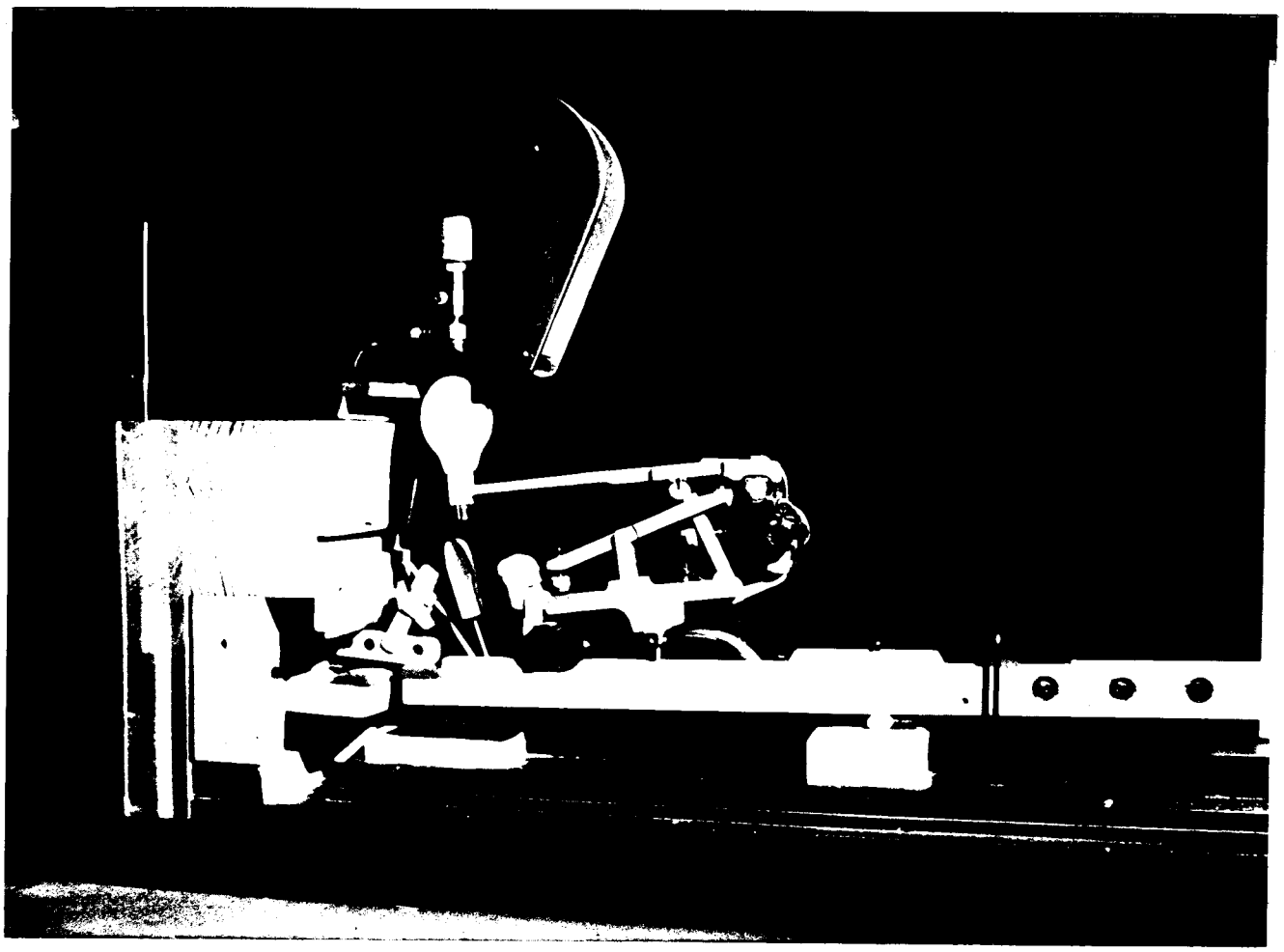

FIG. 1 TEST SETUP USED FOR THE MEASUREMENT

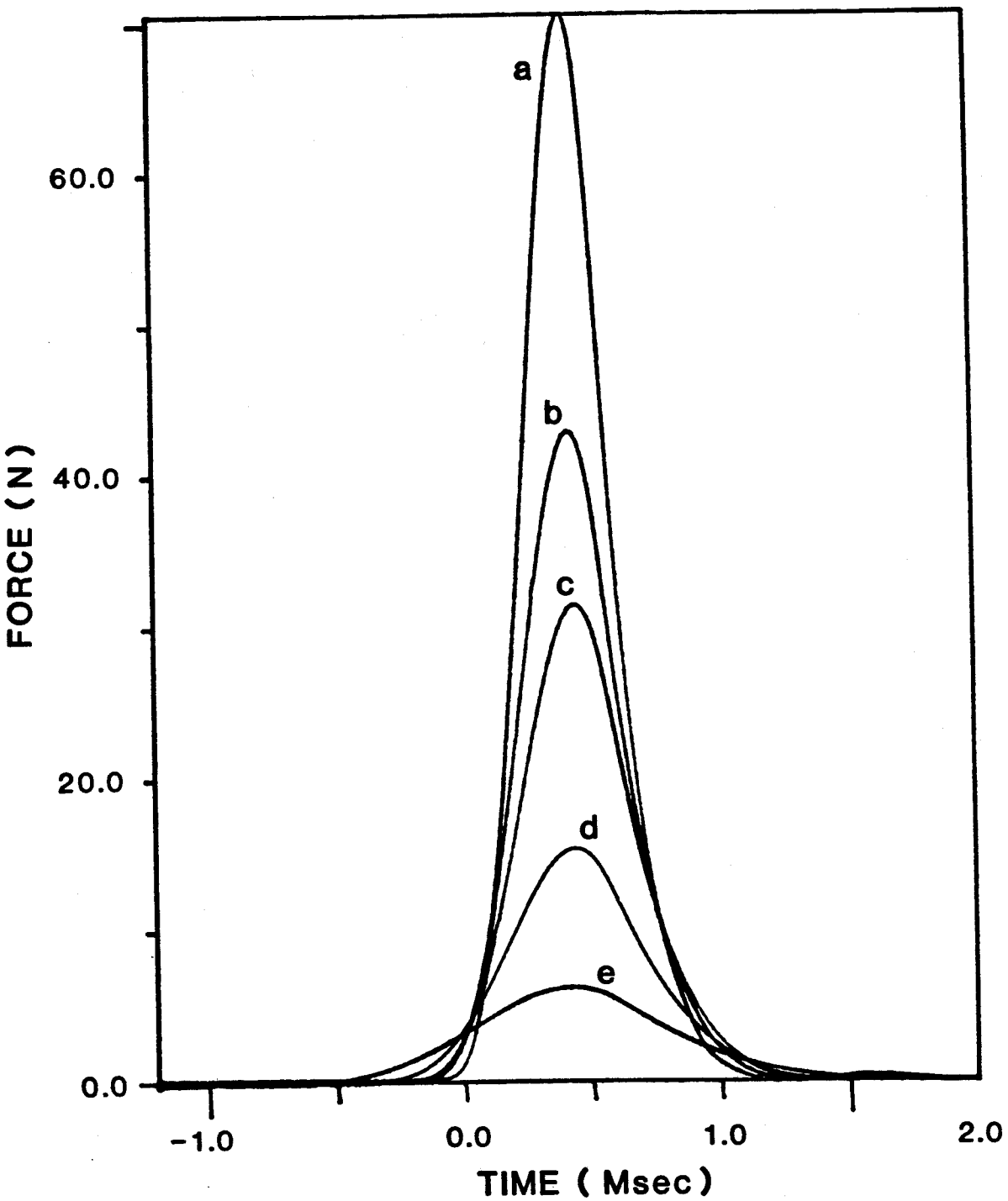

FIG. 2 FORCE-TIME PATTERNS (A-E) FOR DIFFERENT HAMMER SPEEDS.

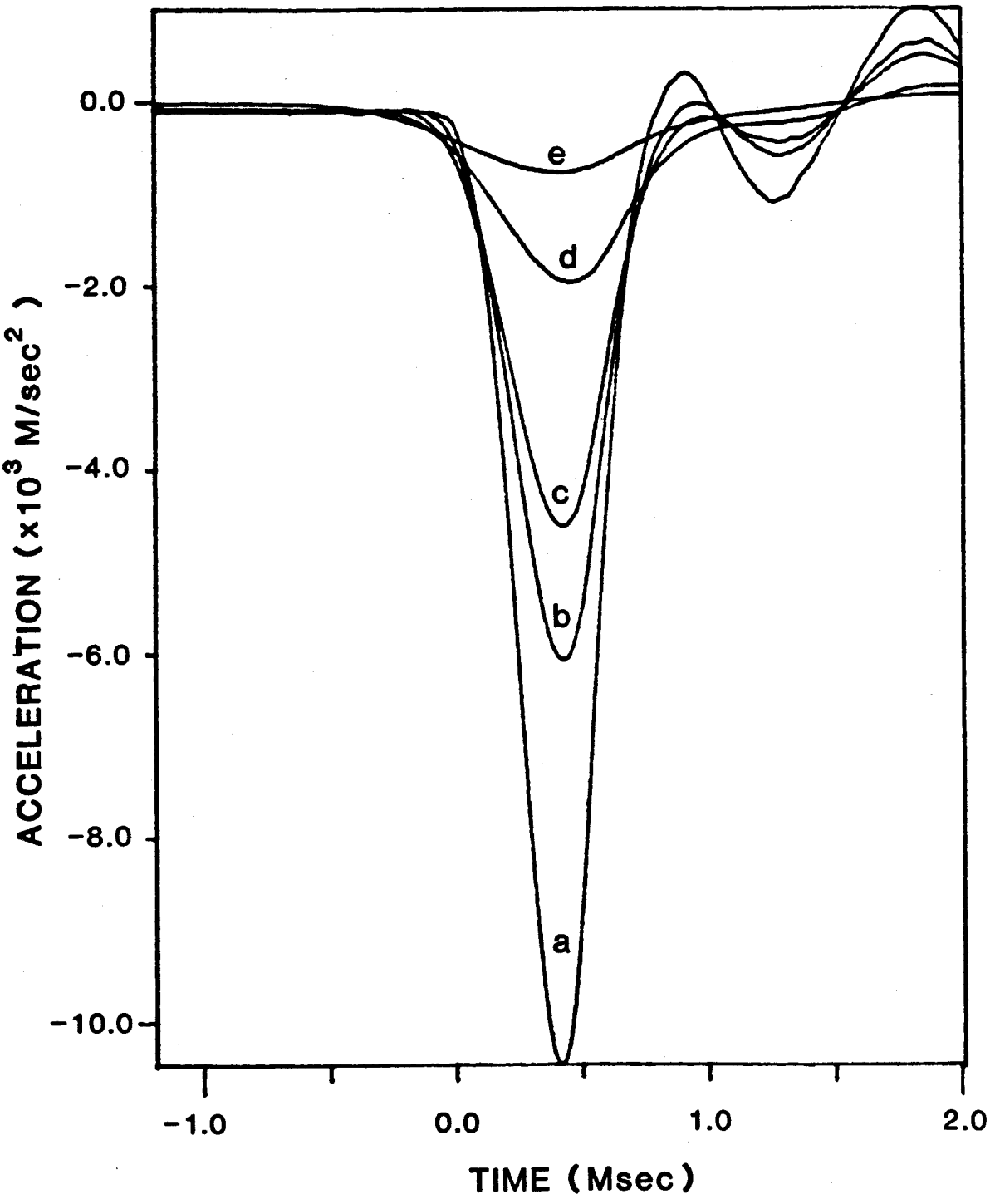

FIG. 3 ACCELERATION-TIME PATTERNS (A-E) FOR DIFFERENT HAMMER SPEEDS.

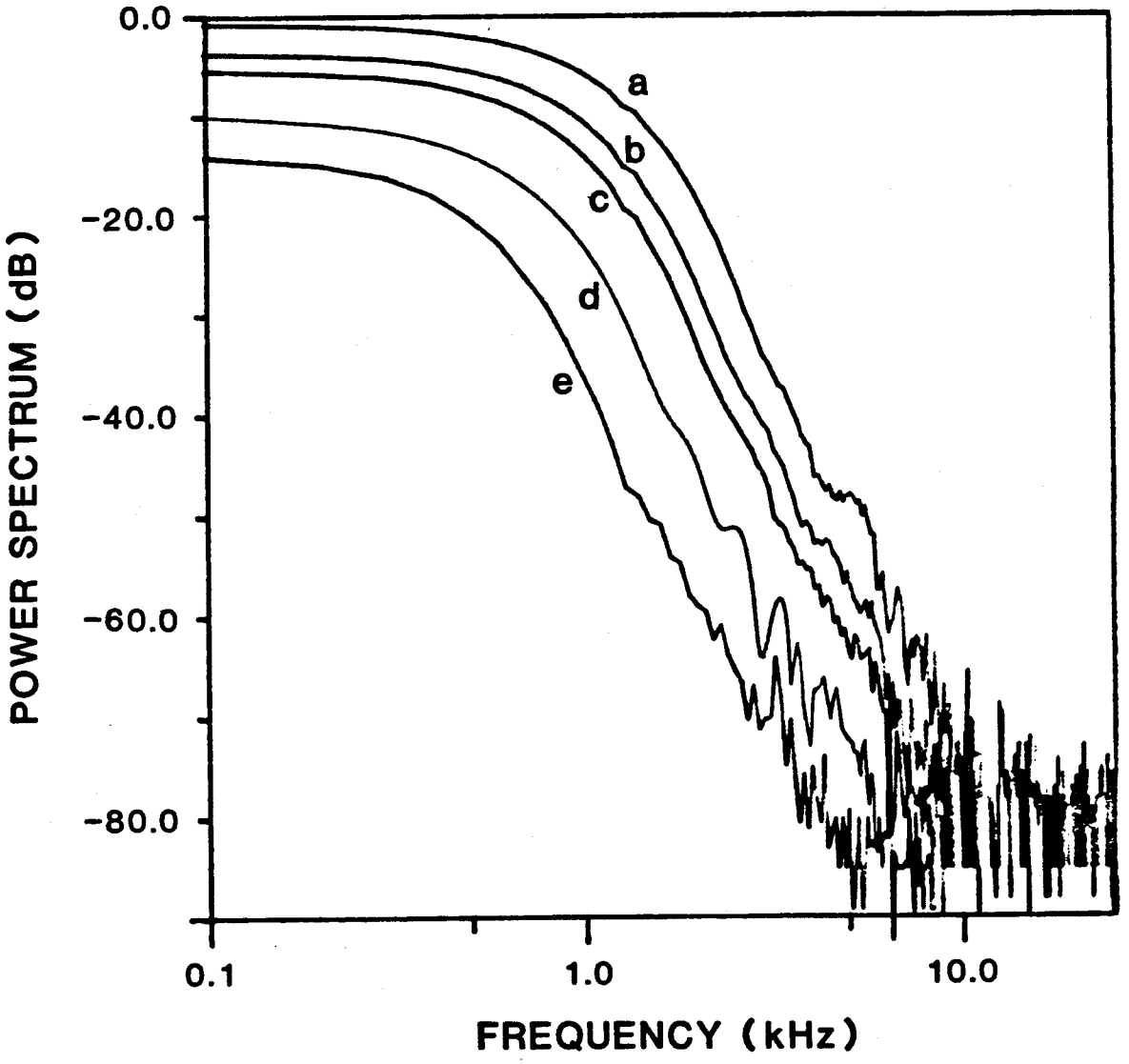

FIG. 4 POWER SPECTRA OF THE FORCE-TIME PATTERNS SHOWN IN FIG. 2

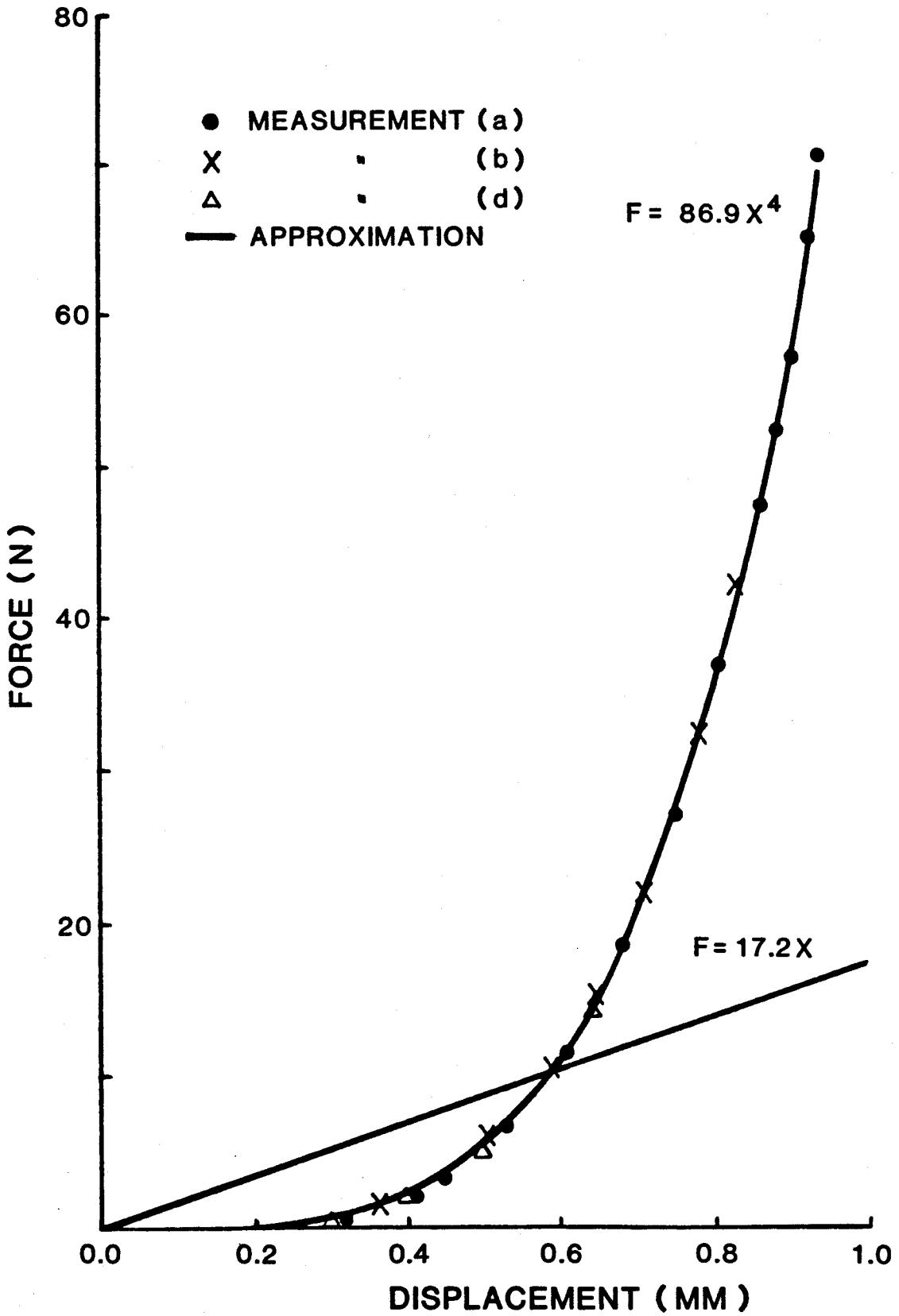

FIG. 5 MEASURED AND SIMULATED FORCE-DISPLACEMENT RELATIONSHIPS

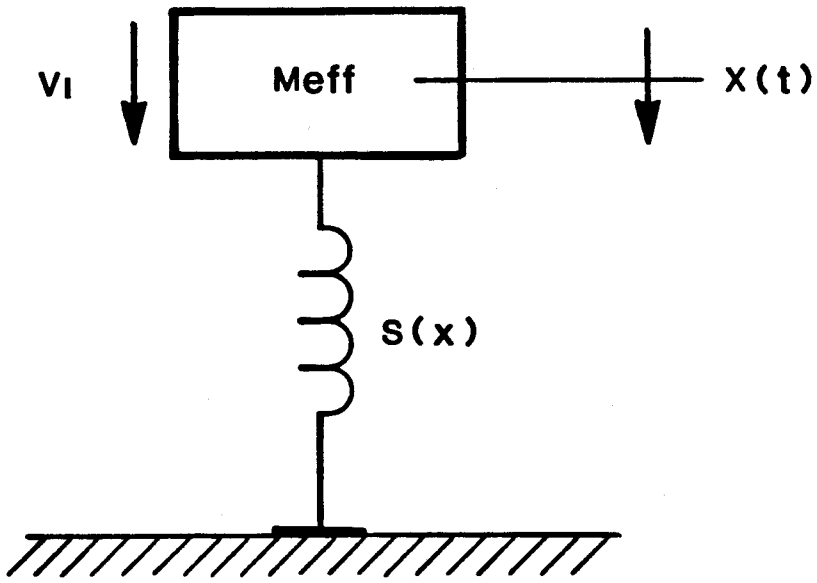

FIG. 6 SINGLE MASS-SPRING MODEL OF A HAMMER

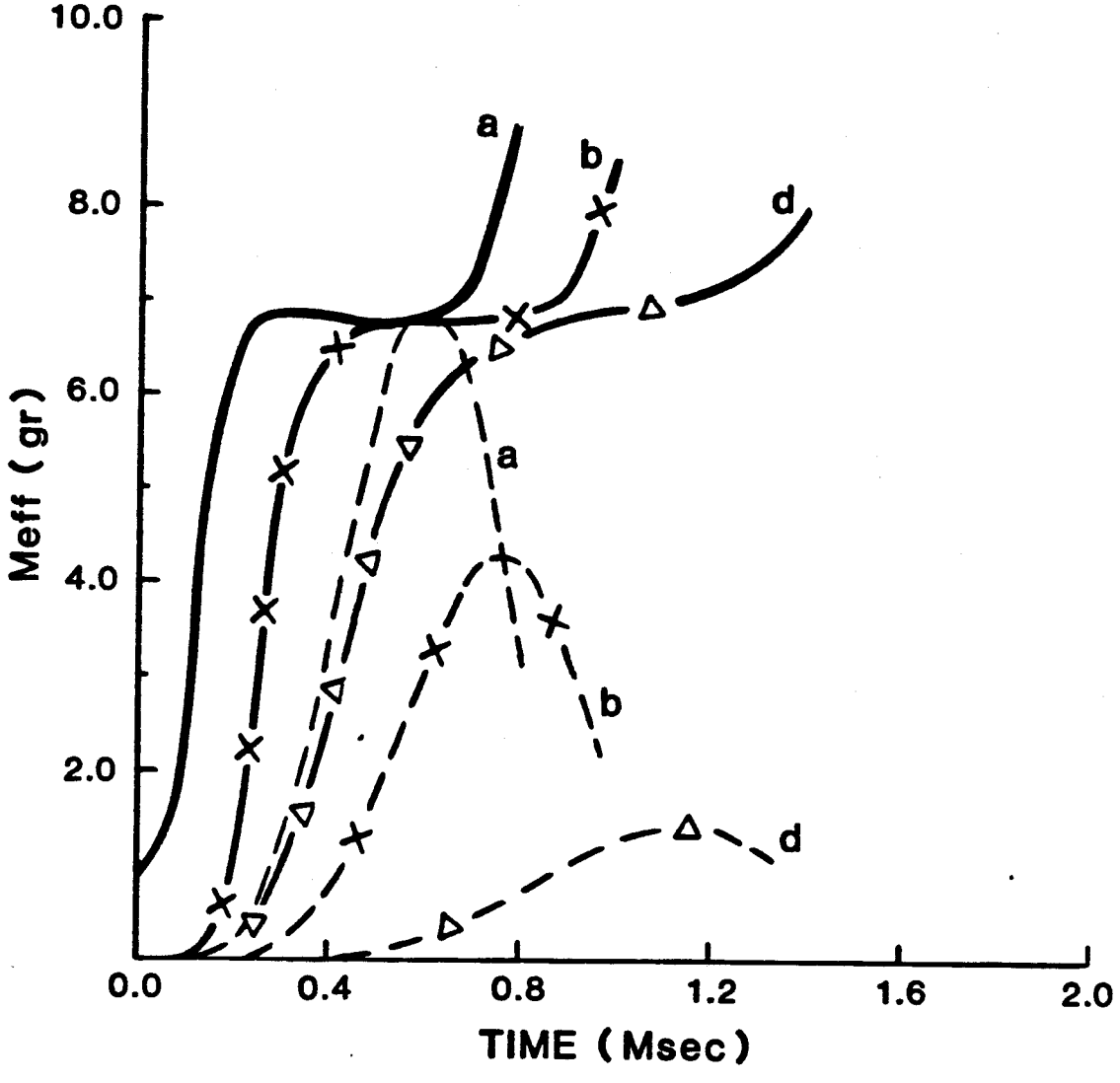

FIG. 7 CALCULATED EFFECTIVE MASSES USING EQ. (4) FOR MEASUREMENTS A, B, AND D (SOLID LINES). THE MEASURED FORCE-TIME PATTERNS ARE ALSO SHOWN (DOTTED LINE).

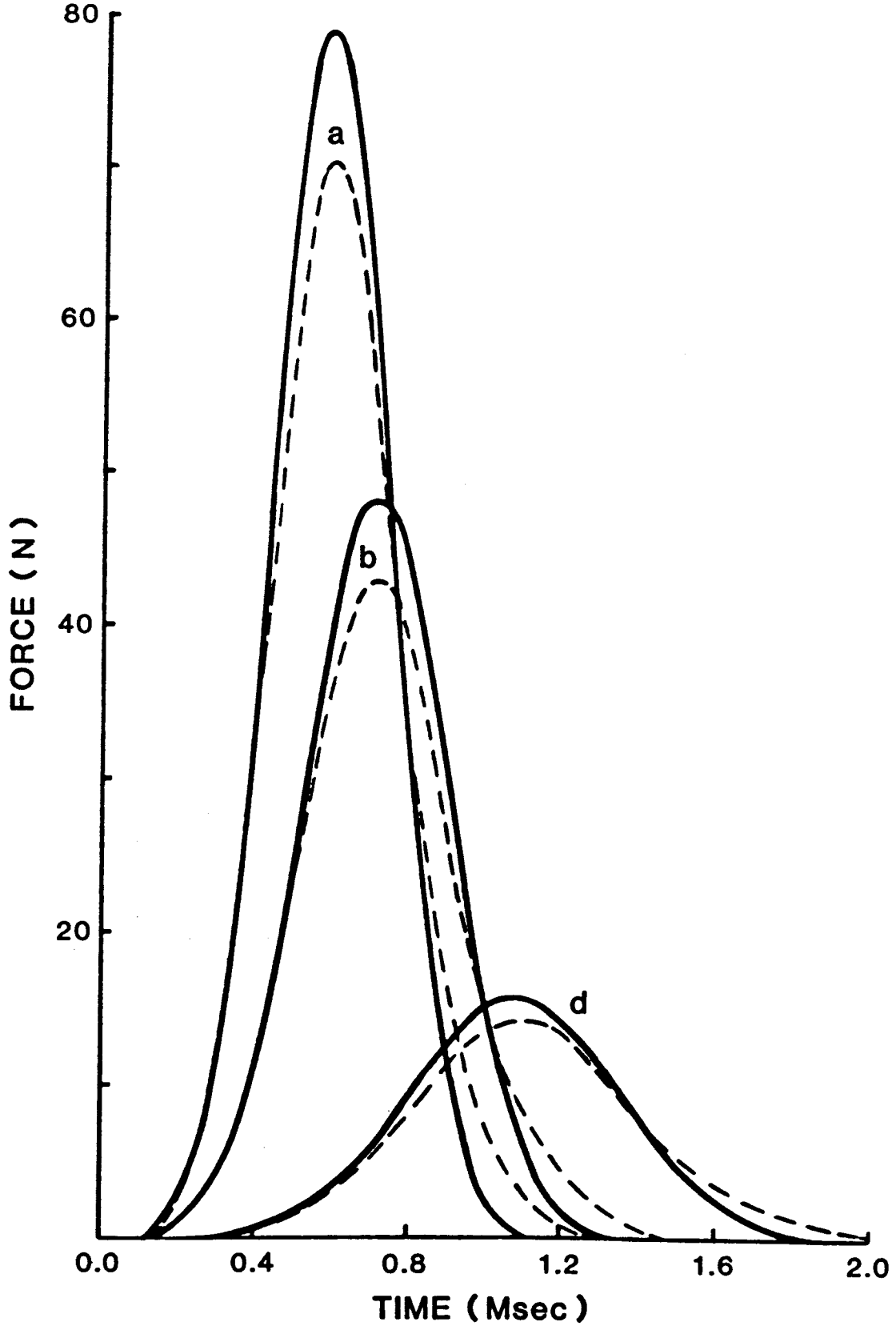

FIG. 8 MEASURED (DOTTED LINE) AND SIMULATED (SOLID LINE) FORCE-TIME PATTERNS FOR MEASUREMENTS A, B, AND D. THE SINGLE MASS-SPRING SYSTEM IS USED AS A HAMMER MODEL.

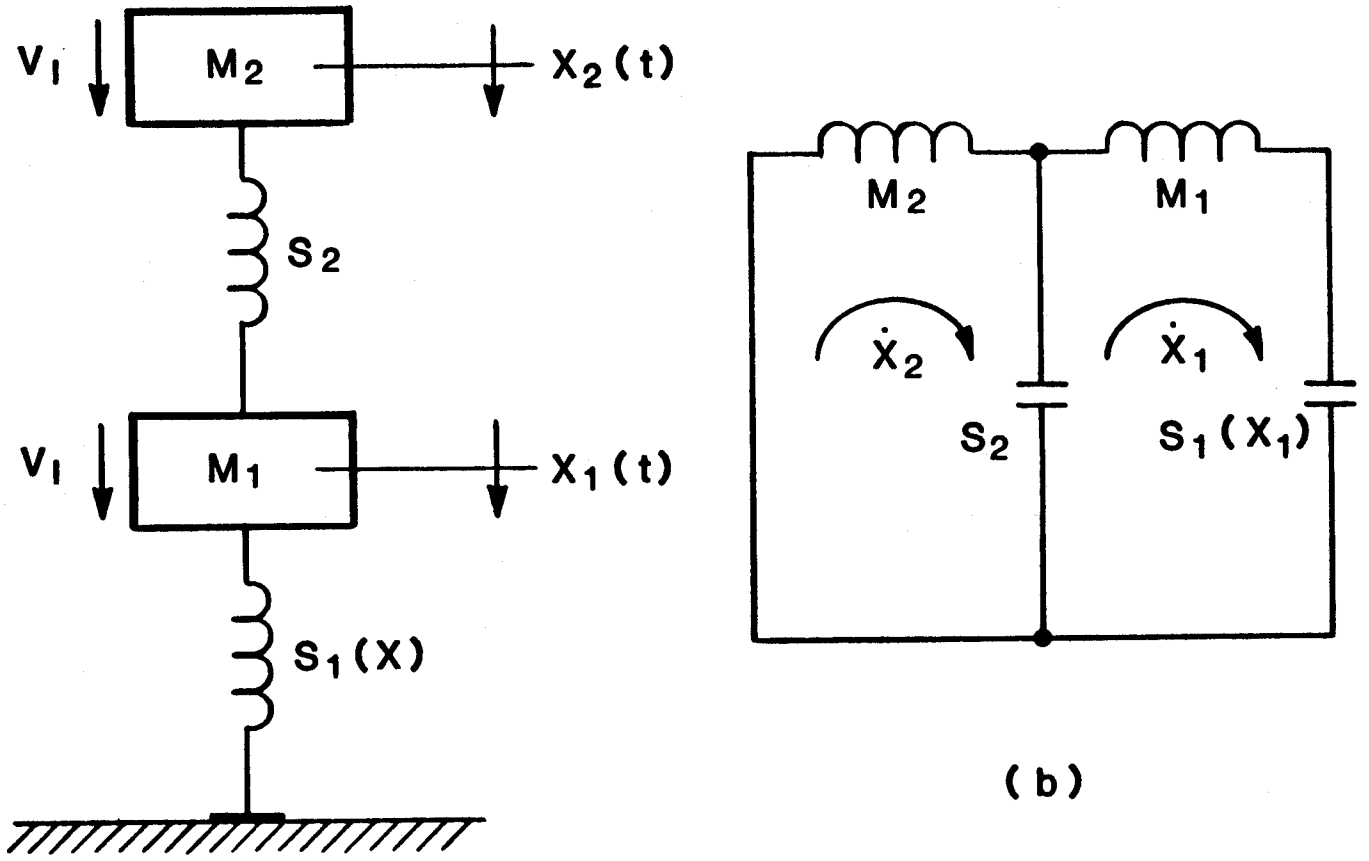

FIG. 9 DOUBLE MASS-SPRING SYSTEM MODEL OF A HAMMER

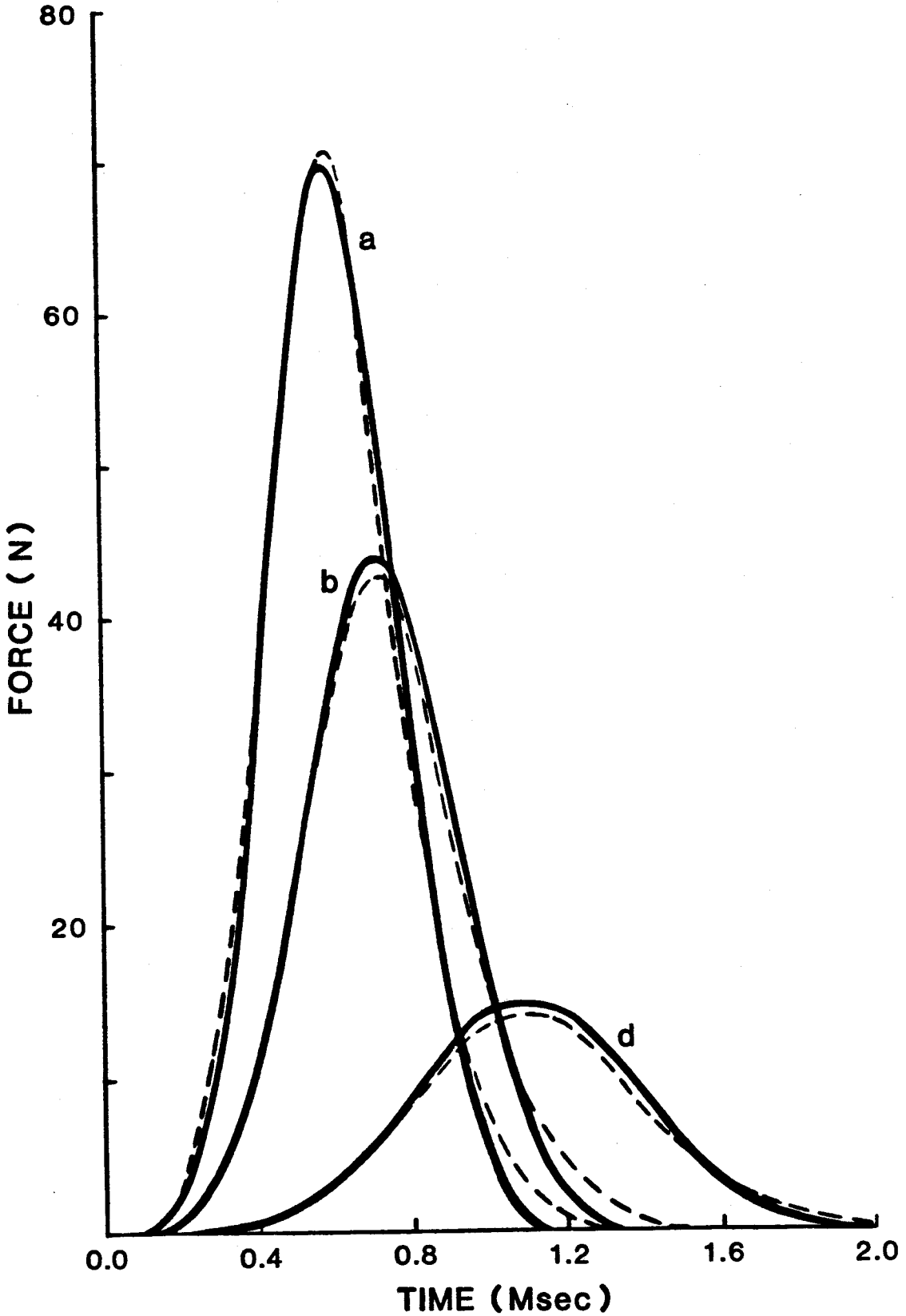

FIG. 10 MEASURED (DOTTED LINE) AND SIMULATED (SOLID LINE) FORCE-TIME PATTERNS FOR MEASUREMENTS A, B, AND D. THE DOUBLE MASS-SPRING SYSTEM IS USED AS A HAMMER MODEL.

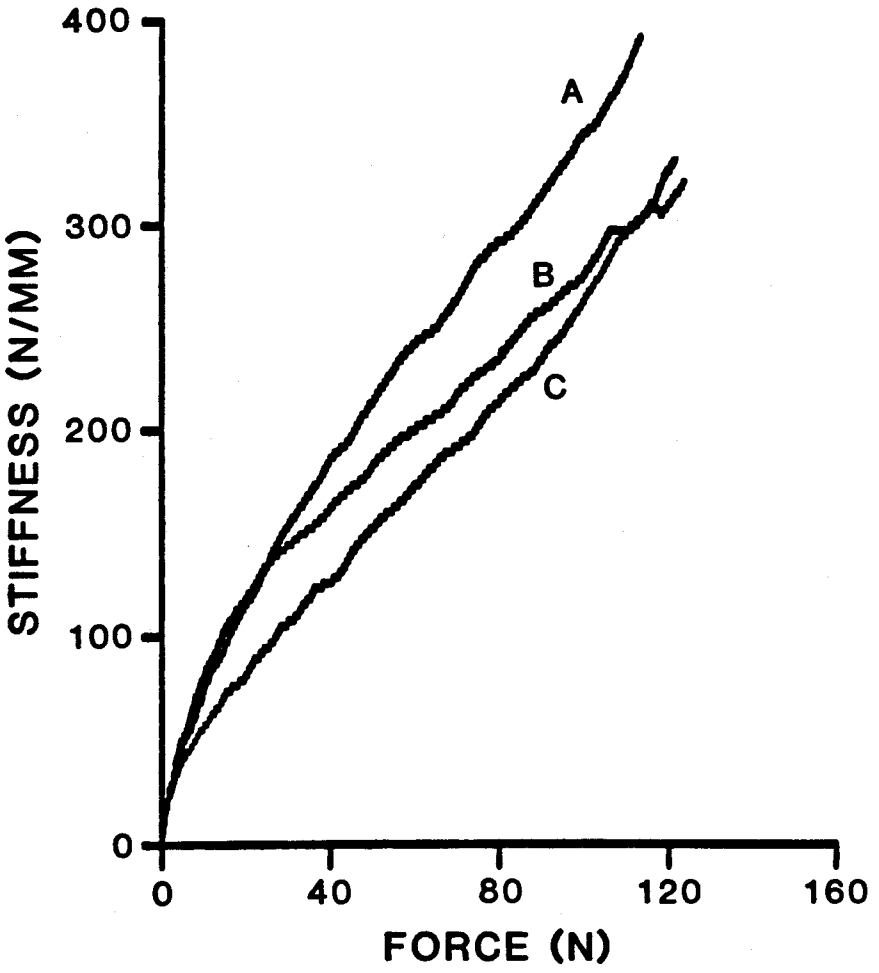

FIG. 11 INCREMENTAL STIFFNESS CRUVES OF THREE DIFFERENT HAMMERS A, B AND C AS A FUNCTION OF FORCE.